Title

Bone-Targeting Exosome Mimetics Engineered by Bioorthogonal Surface Functionalization for Bone Tissue Engineering.

Journal

Nano Letters, 23(4)

Authors

Lee, Chung-Sung
Fan, Jiabing
Hwang, Hee
et al.

Publication Date

2023-02-22

DOI

10.1021/acs.nanolett.2c04159

Peer reviewed

HHS Public Access

Author manuscript

Nano Lett. Author manuscript; available in PMC 2024 February 22.

Published in final edited form as:

Nano Lett. 2023 February 22; 23(4): 1202–1210. doi:10.1021/acs.nanolett.2c04159.

Bone-targeting exosome mimetics engineered by bioorthogonal surface functionalization for bone tissue engineering

Chung-Sung Lee[a,#], **Jiabing Fan**[a,#], **Hee Sook Hwang**[a], **Soyon Kim**[a], **Chen Chen**[a], **Minjee Kang**[a], **Tara Aghaloo**[b], **Aaron W. James**[c,d,*], **Min Lee**[a,e,*]

[a]Division of Advanced Prosthodontics, University of California, Los Angeles, CA 90095, United States

[b]Division of Diagnostic and Surgical Sciences, School of Dentistry, University of California, Los Angeles, CA, 90095, USA

[c]Department of Pathology, School of Medicine, Johns Hopkins University, Baltimore, MD 21205, United States

[d]Orthopedic Hospital Research Center, University of California, Los Angeles, CA 90095, United States

[e]Department of Bioengineering, University of California, Los Angeles, CA 90095, United States

Abstract

Extracellular vesicles have received a great interest as safe biocarriers in biomedical engineering. There is a need to develop more efficient delivery strategies to improve localized therapeutic efficacy and minimize off-target adverse effects. Here, exosome mimetics (EMs) is reported for bone targeting involving the introduction of hydroxyapatite-binding moieties through bioorthogonal functionalization. Bone-binding ability of the engineered EMs is verified with hydroxyapatite-coated scaffolds and an *ex-vivo* bone-binding assay. The EM-bound construct provided a biocompatible substrate for cell adhesion, proliferation, and osteogenic differentiation. Particularly, the incorporation of Smoothened agonist (SAG) into EMs greatly increased the osteogenic capacity through the activation of hedgehog signaling. Furthermore, the scaffold integrated with EM/SAG significantly improved *in vivo* reossification. Lastly, biodistribution studies confirmed the accumulation of systemically administered EMs in bone tissue. This facile engineering strategy could be a versatile tool to promote bone regeneration, offering a promising nanomedicine approach to the sophisticated treatment of bone diseases.

[*]Corresponding authors: **Aaron W. James, MD, PhD**, Professor, Department of Pathology, School of Medicine, Johns Hopkins University, awjames@jhmi.edu, **Min Lee, PhD**, Professor, Division of Advanced Prosthodontics, Department of Bioengineering, University of California, Los Angeles, leemin@ucla.edu.

[#]These authors are contributed equally to this work.

Conflicts of interest

There are no conflicts of interest to declare.

Supporting information

Detailed materials, experimental methods, physicochemical characterization of bone-targeting EMs, western-blot analysis of CD63 and cellular protein in EMs, fluoresence images of FITC-labeled EM-bound mouse femur, confocal fluorescence images of hMSCs stained with calcein AM and ethidium homodimer, relative intensity of staining for RUNX2 and OCN in the immunohistochemical analysis, and biodistibution of bone-targeting EMs *in vivo*.

Graphical Abstract

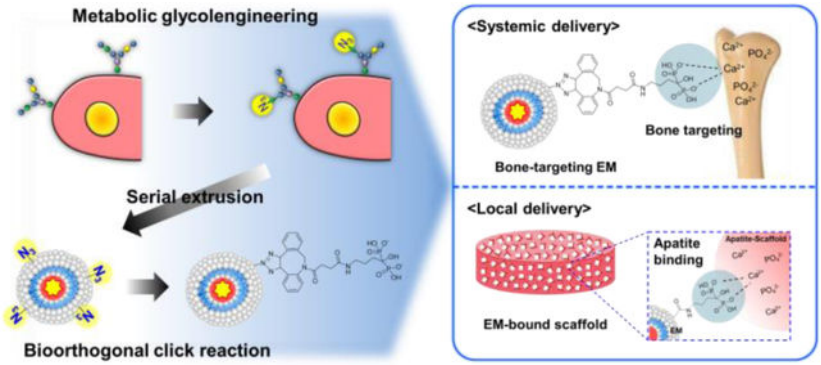

Keywords

Exosome mimetics; click chemistry; bioorthogonal engineering; bone targeting; drug delivery

Cell-free strategies using extracellular vesicles (EVs) or conditioned medium have been garnering attention for properties corresponding with the paracrine effects of stem cells thought to be responsible for their regeneration potential.[1–4] The advantages of approaches involving EVs associated with their intrinsic characteristics include the absence of many problems associated with the use and handling of stem cells, high stability in circulation, low immunogenicity, effective biological activity, ease of storage, and relative affordability compared with cell therapy. These features, then, represent significant improvements over the use of stem cell expansion or the collection of cells from patients.[5–9] Several recent studies have demonstrated the therapeutic value of EVs in musculoskeletal tissue engineering in treating various bone injuries and diseases *in vivo*.[3, 8, 9] Furthermore, EVs are increasingly recognized as a useful nanomaterial for bone tissue engineering.[10, 11] Nonetheless, hurdles relating to the complexity and low yield of the purification process have hindered the widespread therapeutic use of exosomes in clinics. Recently, a relatively simple strategy for the generation of exosome-mimetic (EM) nanovesicles with scalable production yields was developed that relies on the self-assembly of the cellular membrane and internal components resulting from the physical extrusion processes of cell sources.[3, 12]

Nanomaterial-based delivery systems, including EVs, have achieved passive targeting thanks to their extremely small size. Simply put, the ability to move freely through biological barriers provides for the efficient delivery of the vesicles.[13] The modification of the physical or chemical moieties, such as small molecules, peptides, and aptamers, allows for an additional active targeting feature.[14] For the most part, researchers have approached and developed nanomaterial-based targeted delivery as a potential solution to the insufficient therapeutic properties and off-target adverse effects encountered in bone-tissue engineering.[15–17] A novel and safe medical cue with bone-targeting ability, then, is highly desired as a means to reduce the risks associated with off-target adverse effects and increase the efficiency of the treatments for bone injuries and diseases. Because the options currently available for introducing targeting moieties through the delivery of nanomaterials are complex and often depend on chemical reactions that cause non-specific or chemical

modifications, it is difficult to apply them safely to the generation of bone-targeted EVs. For these reasons, researchers and clinicians are eager for a simple and specific technology for generating bone-targeted EVs that can improve the therapeutic efficacy of cell-free medical options.

In recent years, bioorthogonal engineering relying on site-specific copper-free click chemistry as a one-step bioconjugation technique has attracted considerable attention as a fast, biocompatible, and specific reaction in biological systems.[18–21] Bioorthogonal click chemistry has served as an easy and safe strategy for developing advanced targeted delivery systems in various biomedical engineering contexts, especially for cancer treatment.[22–24]

Here, we report engineering of EMs in high yields derived from MSCs, functionalized with bone binding moieties through valuable bioorthogonal reactions, and subsequently integrated onto porous biomaterial scaffolds to develop a cell-free device for bone tissue engineering (Scheme 1). In brief,

1. the metabolic engineering technique displays the azide-modified sialic acid precursors on the cell surface, enabling the introduction of unnatural glycans on the cell surface through the feeding of specific precursors (tetraacetylated N-azidoacetyl-D-mannosamine, Ac_4ManNAz) depending on the intrinsic metabolism;
2. sequential extrusion and purification serve to generate azide-displayed EM (N_3-EM); and
3. a bone-targeting ligand, alendronate (ALD), is functionalized on the EM surface with dibenzocyclooctyne (DBCO) as the clickable material with azide, again through click reaction.

Thus, the final bone-targeting EM (ALD-functionalized EM, ALD-EM) can be immobilized on the hydroxyapatite (HA)-coated 3D bone implant (PLGA scaffold) through binding to the HA surface with high efficiency and extended localization for implantable applications. In addition, the EMs exert intrinsic bone forming ability on its own without drug loading unlike conventional liposomal carriers. Furthermore, the EMs can serve as efficient delivery carriers for therapeutic agents such as, in this study, Smoothened agonist (SAG). SAG can be physically adsorbed onto a scaffold surface but required high doses (>1 mM) for prominent bone formation in our previous study.[25] Thus, this study aims to provide a promising processing strategy to develop a novel cell-free bone graft device releasing drugs that can promote efficacious bone healing. We further confirmed that EMs can serve as bone-targeting delivery carriers in systemic administration because they bind effectively to the HA-rich microenvironment on the bone tissue. This new strategy may be useful for the treatment of local bone defects and systemic bone loss.

First, the hydrodynamic diameter of the EMs was around 20–80 nm, with a narrow distribution (PDI ≤ 0.3) and no significant differences (Figure S1A–E). As shown in transmission electron microscopy (TEM, Figure S1A–D inset), the EMs featured spherical nanostructures and 3D architectures under 100 nm in diameter, a finding consistent with the results of dynamic light scattering. The TEM image and DLS results revealed that the

EMs had sphere-and-single-lamella-type nanostructures with an average size of < 100 nm. Furthermore, the ζ-potential for all types of EMs with or without chemical modifications was negative, approximately −25 mV (Figure S1F). There were no significant changes of these properties after SAG drug loading. We further conducted western blot analysis against CD63 (a specific marker for exosomes) and cellular proteins (Calnexin, Cytochrome c) present in parent hMSCs (Figure S2).[3, 26, 27] The result showed strong expression of CD63 in the EM lysates, indicating that the EMs are exosome analogs. No significant difference in the protein content was observed after chemical modifications or drug loading. Thus, the serial metabolic engineering, bioorthogonal surface modifications, and drug loading did not significantly affect the physicochemical properties of the EMs.

We used confocal laser scanning microscopy (CLSM) to confirm the azide-modified sialic acid precursors on the N_3-EM through metabolic engineering (Figure S1G). The N_3-EMs were incubated with FITC-DBCO conjugates and then further labeled with DiI fluorescence dye, which stains the lipid bilayers, including the EM shell membrane. The CLSM images of N_3-EM clearly showed both green fluorescence (FITC-DBCO) and red fluorescence (DiI) that merged perfectly with a nano-sized sphere shape whereas there was no green fluorescence in the EMs (non-modified EMs) without azide generation. This finding indicates that N_3-EM can easily modify with DBCO-functionalized compounds through the bioorthogonal click reaction between DBCO and azides.

We determined the bone affinity of the ALD-EMs with an *in situ* HA-binding assay using an HA-coated 3D porous PLGA scaffold.[28] The EMs were incubated with the HA-coated 3D PLGA scaffold and then those on the surface of the scaffolds were labeled with Dil dye for fluorescence detection (Figure 1A). The fluorescence images showed a remarkable increase in Dil-labeled EMs resulting from the ALD-EMs bound with HA on the scaffold surface (Figure 1B). In addition, the binding efficacy of the ALD-EMs to HA on the scaffold surface increased over time to 85% of feeding whereas the non-modified EMs and N_3-EMs showed no more than 40%, with the static feature being time-dependent (Figure 1C). These findings demonstrate that the ALD modification of the EM surface through bioorthogonal click chemistry can enhance and facilitate the electrostatic binding of EMs to an HA-rich environment such as bone.

We observed a typical porous morphology with a pore size of around 200–300 μm and a highly interconnected structure in all of the scaffolds (Figure 1D). The HA-PLGA scaffolds showed nubby-textured structures on the surface of the strut. After the functionalization with EMs on the scaffold, no obvious change occurred in the microstructure morphology compared with the morphology of HA-PLGA. The EDX spectra showed that the chemical composition in all types of scaffolds had peaks for calcium (Ca) and phosphorus (P) attributable to the outset layer of HA (Figure 1D). Moreover, the carbon (C) and P peaks of the scaffold with non-modified EMs showed no obvious change because of the low binding capacity of EMs whereas the peaks of the scaffold with the ALD-functionalized EMs, changed dramatically (decreasing for carbon and increasing for phosphorus) by binding the EMs. The *ex vivo* bone-binding results showed a significant rise in the HA-binding of ALD-EMs, where, HA being a major component of the bone microenvironment (Figure 1E and S3). The non-targeted EVs (N_3-EMs) showed no specificity or binding to the HA in

bone. These findings indicate that the ornamentation of ALD plays a significant role in HA binding and targeting the bone microenvironment.

We investigated the osteogenic potential of EMs by evaluating the activity of alkaline phosphatase (ALP), an early osteogenic marker, and mineralization in hMSCs on days 4 and 14, respectively.[29–31] The ALP expression intensified in the presence of EMs, as evidenced by both ALP staining (Figure 2A, upper line) and colorimetric assay (Figure 2B). Furthermore, the ALP activity of the EMs with SAG loading showed the best performance with a significant difference. Consistent with the results of the ALP staining, ALP expression was slightly enhanced with EMs regardless of the presence of ALD. With the EMs containing SAG, expression increased significantly, being approximately 30% greater than with the EMs lacking SAG. The results confirmed similar trends in the mineralization staining (Figure 2A, bottom line) and quantification (Figure 2C). These results indicate that the engineered EM system had a positive effect on the osteogenic differentiation of MSCs and thus has great potential as a bioderived carrier for the delivery of bioactive agents.

The EMs in the presence or absence of ALD modification exhibited approximately 3- and 5-fold higher expression of *ALP* (Figure 2D) and *RUNX2* (Figure 2E) with a significant difference in the quantitative real-time PCR (qRT-PCR) analysis. The gene expression level of OCN showed an approximately 2-fold increase, but this result was not statistically significant (Figure 2F). These gene expression levels in EMs with SAG delivery were higher than those of the control OM (non-treated) and empty EM groups with significant differences. The ALD-EM-SAG showed 4.4-fold, 10.0-fold, and 5.7-fold increase for *ALP*, *RUNX2*, and *OCN*, respectively, compared with the non-treatment group. Overall, exposure to the EMs and delivery of the pro-osteogenic agonist SAG increased gene expression. Moreover, since SAG is known to induce osteogenesis through activation of the hedgehog pathway,[16, 25, 32] we confirmed the function of SAG by monitoring the expression of *PTCH* (Figure 2G) and *GLI1* (Figure 2H), which are hedgehog transcriptional target genes. The qRT-PCR results showed that the expression of both genes for SAG-containing EMs was significantly higher than that of the other groups. The EMs combined with the delivery of SAG as a small molecular activator, then, upregulated the hedgehog signaling, resulting in the enrichment of the osteogenic differentiation of the MSCs.

The engineered scaffold surface with various types of EMs had no significant influence on the adherence or metabolic activity ($p > 0.05$) of the hMSCs (Figure 3A). Furthermore, the cell population on the scaffolds increased over time, demonstrating that the surface engineering with EMs was biocompatible with the proliferation of cells. Most of the MSCs on the scaffolds were stained green and had a spindle shape, indicating that the cells adhered to and spread well on the surface of the scaffold (Figure 3B and Figure S4). These findings suggest that the scaffold with or without the EM immobilization is an excellent substrate for supporting cell attachment, survival, and proliferation after scaffold implantation at the sites of defects.

The scaffolds with EMs displayed intense color development under ALP staining compared with the bare scaffold, indicating that the surface engineering with the EMs promoted the osteogenic differentiation of the hMSCs on the scaffold (Figure 3C). ALP activity

increased significantly in the EM-bound hybrid scaffolds compared with the bare scaffold. Interestingly, the delivery of SAG showed a significantly greater increase than the empty EM-bound hybrid scaffold. In addition, the darkest red color in Alizarin red S staining developed on the EM-bound hybrid scaffolds with SAG delivery (Figure 3D). The results of the quantification inferred from the stained scaffolds showed an increment of mineralized matrix in the EM-bound hybrid scaffold and a further enhancement of the SAG-incorporating hybrid scaffold with a significant difference.

The microCT scanning and quantitative analysis were performed 12 weeks post-implantation to evaluate the bone regeneration capability. A representative 3D reconstructed image of the defect area showed substantially greater regeneration of new bone after the implantation of the scaffolds with EMs than was observed in the control group (Figure 4A). Notably, the EM-bound hybrid scaffold with SAG delivery led to the most effective bone repair with the greatest coverage of the defect site. The new bone area of the SAG-containing EM-bound scaffold (87.6%) and free EM-bound scaffold (64.1%) was dramatically larger than that of the bare scaffold (38.6%) (Figure 4B). The SAG-containing group resulted in a remarkable increase with a statistical significance in the bone volume density compared with the other experimental groups (Figure 4C). Moreover, the bone mineral density of the EM-bound hybrid scaffold was significantly promoted, and even higher bone volume density was observed in the SAG-containing group (Figure 4D). In addition, though there was no significant improvement in the free EM-bound hybrid scaffold compared with the bare scaffold control, the density of the regenerated bone in the SAG-containing EM-bound hybrid scaffold was noticeable, as evidenced by the evaluation of trabecular number (Figure 4E). These findings suggest that the EM-engineered hybrid scaffold exhibits excellent performance in the re-ossification of bone defects since EMs can act as an effective osteogenic activator and delivery vector for osteoinductive agents and, therefore, is a promising strategy for bone repair.

We also performed histological evaluations through a series of stains, including H&E, Masson’s trichrome, and Picrosirius red staining (Figure 4F). The defects in the control bare scaffold showed in-growth at the edge of the parietal bone and adjacent fibrous tissue, but we observed mature new bone clearly in the EM-bound hybrid scaffold. The implantation of the SAG-containing groups resulted in the thickest bony structure that we observed at the center as well as the junction of the defects, as evidenced by staining with H&E and Masson’s trichrome. In addition, we detected the development and distribution of collagen in the defects with Picrosirius red staining to demonstrate the quality of the regenerated bone.[33] We observed a high level of mixed birefringence (yellow- and green-colored regions) over a large area of the collagen matrices in the SAG-containing group, suggesting that the regenerated bone tissue was comparable to native mature bone, whereas there were only a few signals in the bare scaffold and free EM-bound hybrid scaffold.

We observed low or moderate expression of RUNX2, and the expression of OCN was especially strong on the bare or free EM-bound hybrid scaffold in immunohistochemical staining, respectively (Figure 4G and S5). The darkest brown signals in both the RUNX2 and OCN staining in the osteoblasts and osteocytes appeared along the regenerated bone area in the SAG-containing group. This result indicates that the biomaterial scaffold with

EM application and stimulation by SAG delivery promotes the osteoinductive capacity for efficacious bone healing.

We assessed the bone-homing capacity of EMs by performing *in vivo* biodistribution using fluorescence dye-encapsulated EMs tracked with an *in vivo* imaging system in CD-1 nude mice after intravenous injection through the tail vein (Figure S6A). Though the fluorescence signals were gradually enhanced over time in both experimental groups, the signals for bone-targeted EMs (ALD-EMs) were clearly higher than those of the control EMs at all time points. At 48 h post-administration, the retention of the ALD-modified EMs increased dramatically in the whole body compared with the non-modified EMs. We quantified the total radiance of the mouse body images, and the results showed increased retention of the targeted EMs with a significant difference compared with the non-targeted EMs (Figure S6B). An *ex vivo* analysis showed targeted EMs accumulated at high levels in the skull, mandibles, and femurs at 24 and 48 h post-injection (Figure S6C). The fluorescence signals of the targeted EMs in the organs, except bony tissues, were rarely observed. The radiance of the *ex vivo* fluorescence images strongly supported the findings of bone-targeting and high retention capacities in the bone tissue of the targeted EMs (Figure S6D). Thus, the *in vivo* biodistribution studies supported the results presented above for the EM-binding hybrid scaffold, and they highlight the potential of EMs engineered by bioorthogonal click reaction for systemic bone-targeting to treat systemic bone diseases, including osteoporosis. Furthermore, the bone-targeting feature indicates that the EMs released from the EM-bound scaffolds after implantation into the defect can help to localize the EMs successfully at the defect sites as a result of specific interactions between the bisphosphonate on the EMs and the calcium on the natural bone. Further study will investigate therapeutic efficacy against systemic bone diseases, such as osteoporosis, after systemic administration. Pharmacokinetic analysis including *in vivo* distribution, metabolism, and excretion of our EMs will be further conducted in future studies.

In summary, we successfully developed cell-derived, bone-targeting nanovesicles, known as exosome mimetics (EMs), through surface engineering with bioorthogonal chemistry for use in bone-tissue engineering. The bone-targeting EMs showed excellent binding affinity to the artificial and natural apatite substrates for the bone. We fabricated an EM-bound 3D hybrid scaffold with good bone-binding affinity that provides a biocompatible substrate for cell adhesion, survival, proliferation, and osteogenic potential. Furthermore, the EMs played a critical role as a delivery carrier of bioactive compounds, such as Smoothened agonist SAG, which activates hedgehog signaling. The engineered hybrid scaffold with SAG-containing EM showed promising osteogenic and reossification potential *in vitro* and *in vivo*. Additionally, the targeted EMs displayed considerable capacity for the systemic targeting of various bone tissues in the biodistribution study. Thus, targeted EMs engineered by bioorthogonal chemistry show promise as an easy-to-use tool for modifying the bone microenvironment and promoting bone regeneration.

Supplementary Material

Refer to Web version on PubMed Central for supplementary material.

Acknowledgements

C.-S.L. and J.F. are contributed equally to this work. Present address for C.-S.L. is Department of Pharmaceutical Engineering, Soonchunhyang University, Asan 31538, Republic of Korea. Present address for H.S.H. is Department of Pharmaceutical Engineering, Dankook University, Cheonan 31116, Republic of Korea. This work was supported by grants from the National Institutes of Health (R01 DE027332 and R01 DE031711), the Department of Defense (W81XWH-18-1-0337), and the MTF Biologics.

References

(1). Gnecchi M; He H; Liang OD; Melo LG; Morello F; Mu H; Noiseux N; Zhang L; Pratt RE; Ingwall JS Paracrine action accounts for marked protection of ischemic heart by Akt-modified mesenchymal stem cells. Nature medicine 2005, 11 (4), 367–368.

(2). Nakamura Y; Miyaki S; Ishitobi H; Matsuyama S; Nakasa T; Kamei N; Akimoto T; Higashi Y; Ochi M Mesenchymal-stem-cell-derived exosomes accelerate skeletal muscle regeneration. FEBS letters 2015, 589 (11), 1257–1265. [PubMed: 25862500]

(3). Fan J; Lee C-S; Kim S; Chen C; Aghaloo T; Lee M Generation of small RNA-modulated exosome mimetics for bone regeneration. ACS nano 2020, 14 (9), 11973–11984. [PubMed: 32897692]

(4). Zha Y; Lin T; Li Y; Zhang X; Wang Z; Li Z; Ye Y; Wang B; Zhang S; Wang J Exosome-mimetics as an engineered gene-activated matrix induces in-situ vascularized osteogenesis. Biomaterials 2020, 247, 119985. [PubMed: 32272301]

5. Herberts CA; Kwa MS; Hermsen HP Risk factors in the development of stem cell therapy. Journal of translational medicine 2011, 9 (1), 1–14.

6. Fan M; Chen W; Liu W; Du G-Q; Jiang S-L; Tian W-C; Sun L; Li R-K; Tian H The effect of age on the efficacy of human mesenchymal stem cell transplantation after a myocardial infarction. Rejuvenation research 2010, 13 (4), 429–438. [PubMed: 20583954]

7. Vizoso FJ; Eiro N; Cid S; Schneider J; Perez-Fernandez R Mesenchymal stem cell secretome: toward cell-free therapeutic strategies in regenerative medicine. International journal of molecular sciences 2017, 18 (9), 1852. [PubMed: 28841158]

8. Marolt Presen D; Traweger A; Gimona M; Redl H Mesenchymal stromal cell-based bone regeneration therapies: from cell transplantation and tissue engineering to therapeutic secretomes and extracellular vesicles. Frontiers in bioengineering and biotechnology 2019, 7, 352. [PubMed: 31828066]

9. Kang M; Lee C-S; Lee M Bioactive scaffolds integrated with liposomal or extracellular vesicles for bone regeneration. Bioengineering 2021, 8 (10), 137. [PubMed: 34677210]

10. Batrakova EV; Kim MS Using exosomes, naturally-equipped nanocarriers, for drug delivery. Journal of Controlled Release 2015, 219, 396–405. [PubMed: 26241750]

11. El-Andaloussi S; Lee Y; Lakhal-Littleton S; Li J; Seow Y; Gardiner C; AlvarezErviti L; Sargent IL; Wood MJ Exosome-mediated delivery of siRNA in vitro and in vivo. Nature protocols 2012, 7 (12), 2112–2126. [PubMed: 23154783]

12. Yoon JK; Kim DH; Kang ML; Jang HK; Park HJ; Lee JB; Yi SW; Kim HS; Baek S; Park DB Anti-Atherogenic Effect of Stem Cell Nanovesicles Targeting Disturbed Flow Sites. Small 2020, 16 (16), 2000012.

13. Jiang W; Kim BY; Rutka JT; Chan WC Nanoparticle-mediated cellular response is size-dependent. Nature nanotechnology 2008, 3 (3), 145–150.

14. Lee D-E; Koo H; Sun I-C; Ryu JH; Kim K; Kwon IC Multifunctional nanoparticles for multimodal imaging and theragnosis. Chemical Society Reviews 2012, 41 (7), 2656–2672. [PubMed: 22189429]

15. Cheng H; Chawla A; Yang Y; Li Y; Zhang J; Jang HL; Khademhosseini A Development of nanomaterials for bone-targeted drug delivery. Drug Discovery Today 2017, 22 (9), 1336–1350. [PubMed: 28487069]

16. Lee C-S; Hsu GC-Y; Sono T; Lee M; James AW Development of a biomaterial scaffold integrated with osteoinductive oxysterol liposomes to enhance Hedgehog signaling and bone repair. Molecular Pharmaceutics 2021, 18 (4), 1677–1689. [PubMed: 33760625]

17. Lee C-S; Kim S; Fan J; Hwang HS; Aghaloo T; Lee M Smoothened agonist sterosome immobilized hybrid scaffold for bone regeneration. Science advances 2020, 6 (17), eaaz7822. [PubMed: 32494652]
18. Yoon HI; Yhee JY; Na JH; Lee S; Lee H; Kang S-W; Chang H; Ryu JH; Lee S; Kwon IC Bioorthogonal copper free click chemistry for labeling and tracking of chondrocytes in vivo. Bioconjugate chemistry 2016, 27 (4), 927–936. [PubMed: 26930274]
19. Dean KM; Palmer AE Advances in fluorescence labeling strategies for dynamic cellular imaging. Nature chemical biology 2014, 10 (7), 512–523. [PubMed: 24937069]
20. Ramil CP; Lin Q Bioorthogonal chemistry: strategies and recent developments. Chemical communications 2013, 49 (94), 11007–11022. [PubMed: 24145483]
21. Koo H; Lee S; Na JH; Kim SH; Hahn SK; Choi K; Kwon IC; Jeong SY; Kim K Bioorthogonal copper-free click chemistry in vivo for tumor-targeted delivery of nanoparticles. Angewandte Chemie 2012, 124 (47), 12006–12010.
22. Kang S-W; Lee S; Na JH; Yoon HI; Lee D-E; Koo H; Cho YW; Kim SH; Jeong SY; Kwon IC Cell labeling and tracking method without distorted signals by phagocytosis of macrophages. Theranostics 2014, 4 (4), 420. [PubMed: 24578725]
23. Hart C; Chase LG; Hajivandi M; Agnew B Metabolic labeling and click chemistry detection of glycoprotein markers of mesenchymal stem cell differentiation. In Mesenchymal Stem Cell Assays and Applications, Springer, 2011; pp 459–484.
24. Lee S; Koo H; Na JH; Han SJ; Min HS; Lee SJ; Kim SH; Yun SH; Jeong SY; Kwon IC Chemical tumor-targeting of nanoparticles based on metabolic glycoengineering and click chemistry. ACS nano 2014, 8 (3), 2048–2063. [PubMed: 24499346]
25. Lee S; Shen J; Pan HC; Shrestha S; Asatrian G; Nguyen A; Meyers C; Nguyen V; Lee M; Soo C Calvarial defect healing induced by small molecule smoothened agonist. Tissue Engineering Part A 2016, 22 (23–24), 1357–1366. [PubMed: 27702396]
26. Mathieu M; Martin-Jaular L; Lavieu G; Théry C Specificities of secretion and uptake of exosomes and other extracellular vesicles for cell-to-cell communication. Nature cell biology 2019, 21 (1), 9–17. [PubMed: 30602770]
27. Feng T; Karges J; Liao X; Ji L; Chao H Engineered exosomes as a natural nanoplatform for cancer targeted delivery of metal-based drugs. Coordination Chemistry Reviews 2022, 454, 214325.
28. Zhang X; Fan J; Lee CS; Kim S; Chen C; Aghaloo T; Lee M Apatite-binding nanoparticulate agonist of hedgehog signaling for bone repair. Advanced functional materials 2020, 30 (12), 1909218. [PubMed: 32952492]
29. Kim S; Fan J; Lee C-S; Chen C; Lee M Sulfonate Hydrogel–siRNA Conjugate Facilitates Osteogenic Differentiation of Mesenchymal Stem Cells by Controlled Gene Silencing and Activation of BMP Signaling. ACS Applied Bio Materials 2021, 4 (6), 5189–5200.
30. Lee CS; Hwang HS; Kim S; Fan J; Aghaloo T; Lee M Inspired by nature: facile design of nanoclay–organic hydrogel bone sealant with multifunctional properties for robust bone regeneration. Advanced functional materials 2020, 30 (43), 2003717. [PubMed: 33122980]
31. Kim S; Fan J; Lee C-S; Chen C; Bubukina K; Lee M Heparinized chitosan stabilizes the bioactivity of BMP-2 and potentiates the osteogenic efficacy of demineralized bone matrix. Journal of biological engineering 2020, 14 (1), 1–12. [PubMed: 31956340]
32. Lee S; Wang C; Pan HC; Shrestha S; Meyers C; Ding C; Shen J; Chen E; Lee M; Soo C Combining Smoothened Agonist (SAG) and NEL-like protein-1 (NELL-1) Enhances Bone Healing. Plastic and reconstructive surgery 2017, 139 (6), 1385. [PubMed: 28198775]
33. Kim S; Fan J; Lee C-S; Lee M Dual functional lysozyme–chitosan conjugate for tunable degradation and antibacterial activity. ACS applied bio materials 2020, 3 (4), 2334–2343.

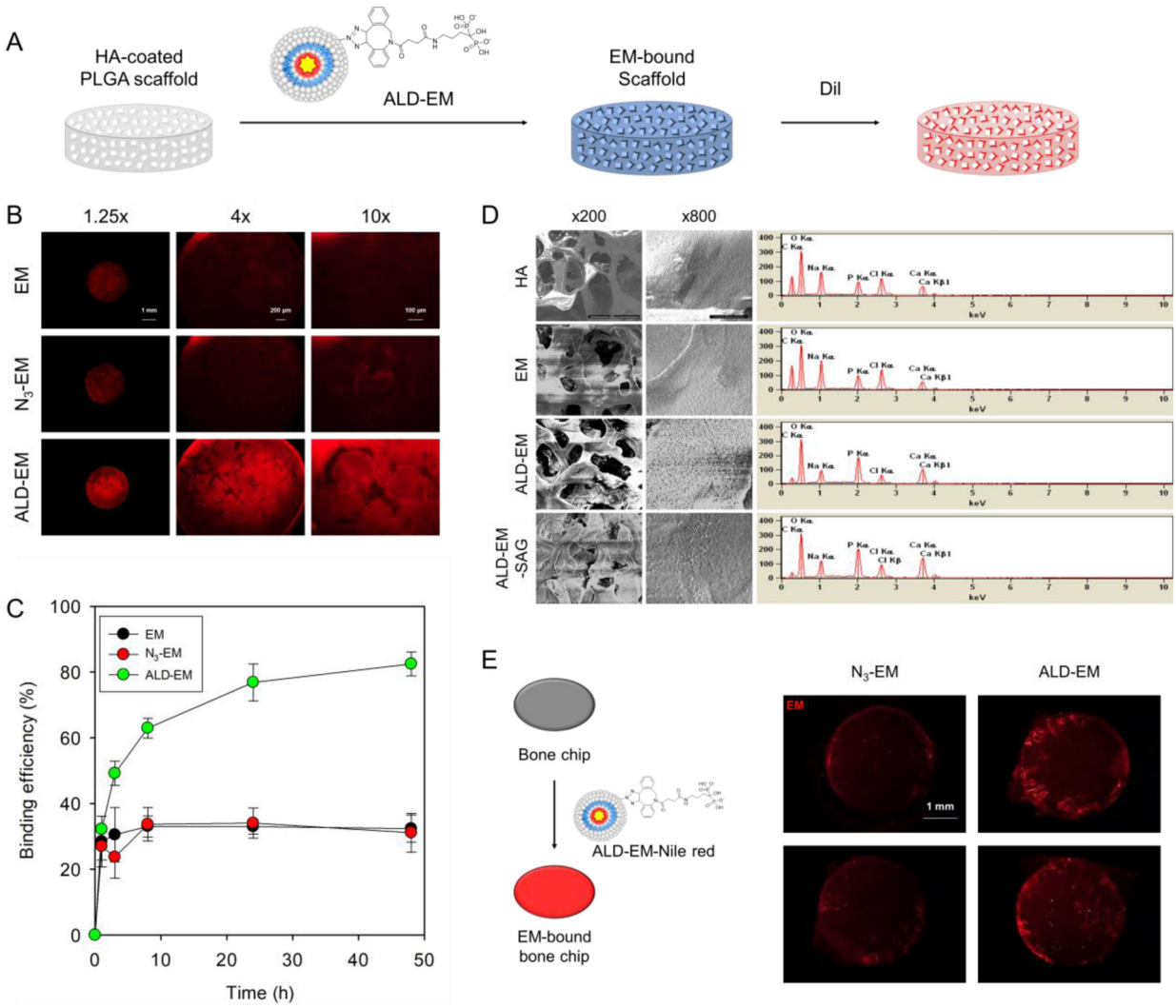

Figure 1. Binding ability of bone-targeting exosome mimetics on the HA-coated PLGA scaffold and mouse skull bone (*ex vivo*).

A) Schematic illustration of the bone-binding experiment with the HA-coated PLGA scaffold. B) Fluorescence images of EM-bound PLGA scaffolds after incubating for 24 h and staining with Dil dye. C) The binding kinetics of various EMs to the HA surface at various incubating times (means ± standard deviation, n = 3). D) SEM images and EDX spectra of various surfaces (HA, EM, ALD-EM, and ALD-EM-SAG). The scale bar indicates 400 and 50 μm for low and high magnification images, respectively. E) Schematic illustration of *ex vivo* bone-binding experiment with a mouse skull bone chip with nile red-loaded ALD-EMs and fluorescence images of EM-bound bone chips.

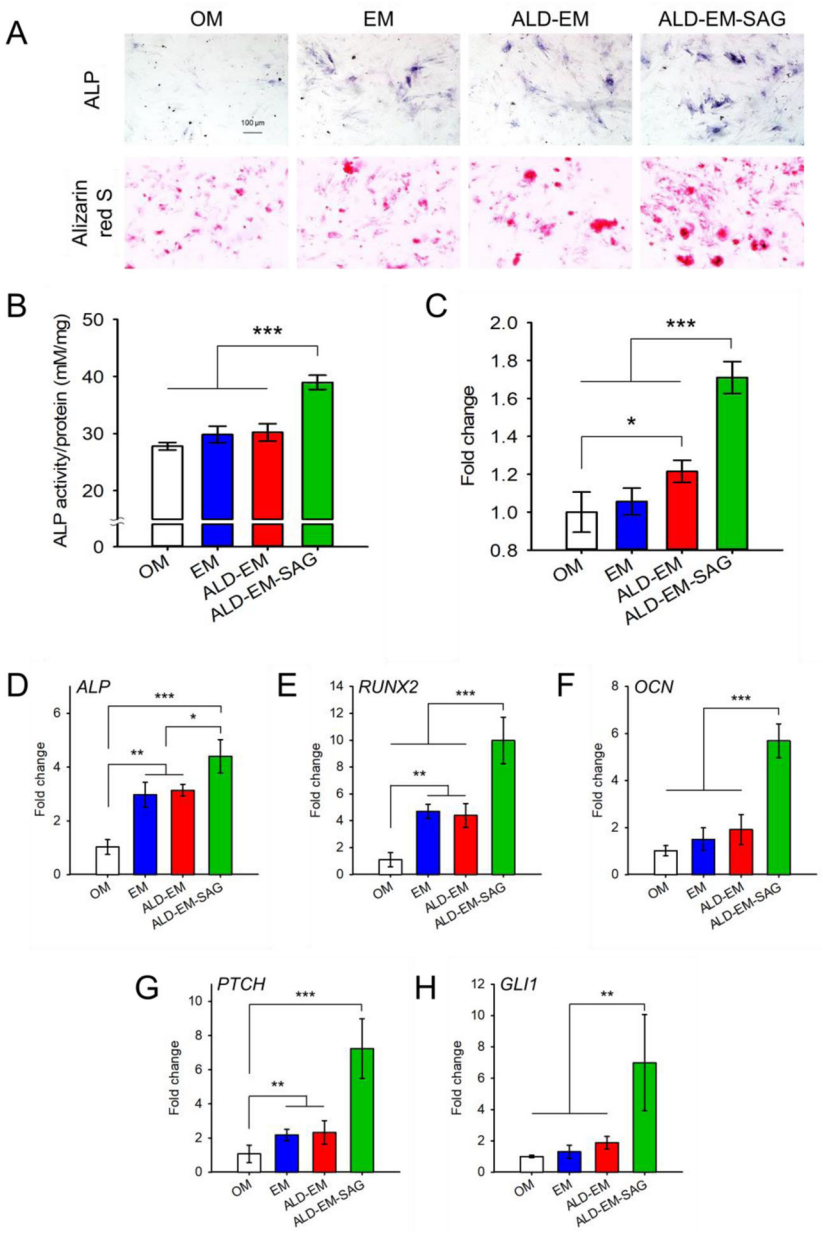

Figure 2. Osteoinductive activity of EMs in 2D cell culture.

A, top line) ALP staining and B) ALP activity were performed and determined on day 4. A, bottom line) Alizarin red S staining was carried out on day 14, and C) quantification was also evaluated. The scale bars indicate 100 μm in A). Error bars indicate standard deviations (three independent cultures; n = 3). The gene expression related to osteogenesis and hedgehog signaling was evaluated with qRT-PCR. D) *ALP* and E) *RUNX2* were examined on day 4, and F) *OCN* was measured on day 14 for osteogenesis. G) *PTCH* and H) *GLI1* were examined on day 4 for hedgehog signaling. The error bars indicate standard deviations ($n = 3$); *$p < 0.05$, **$p < 0.01$, and ***$p < 0.001$ (ANOVA followed by Tukey's post hoc test).

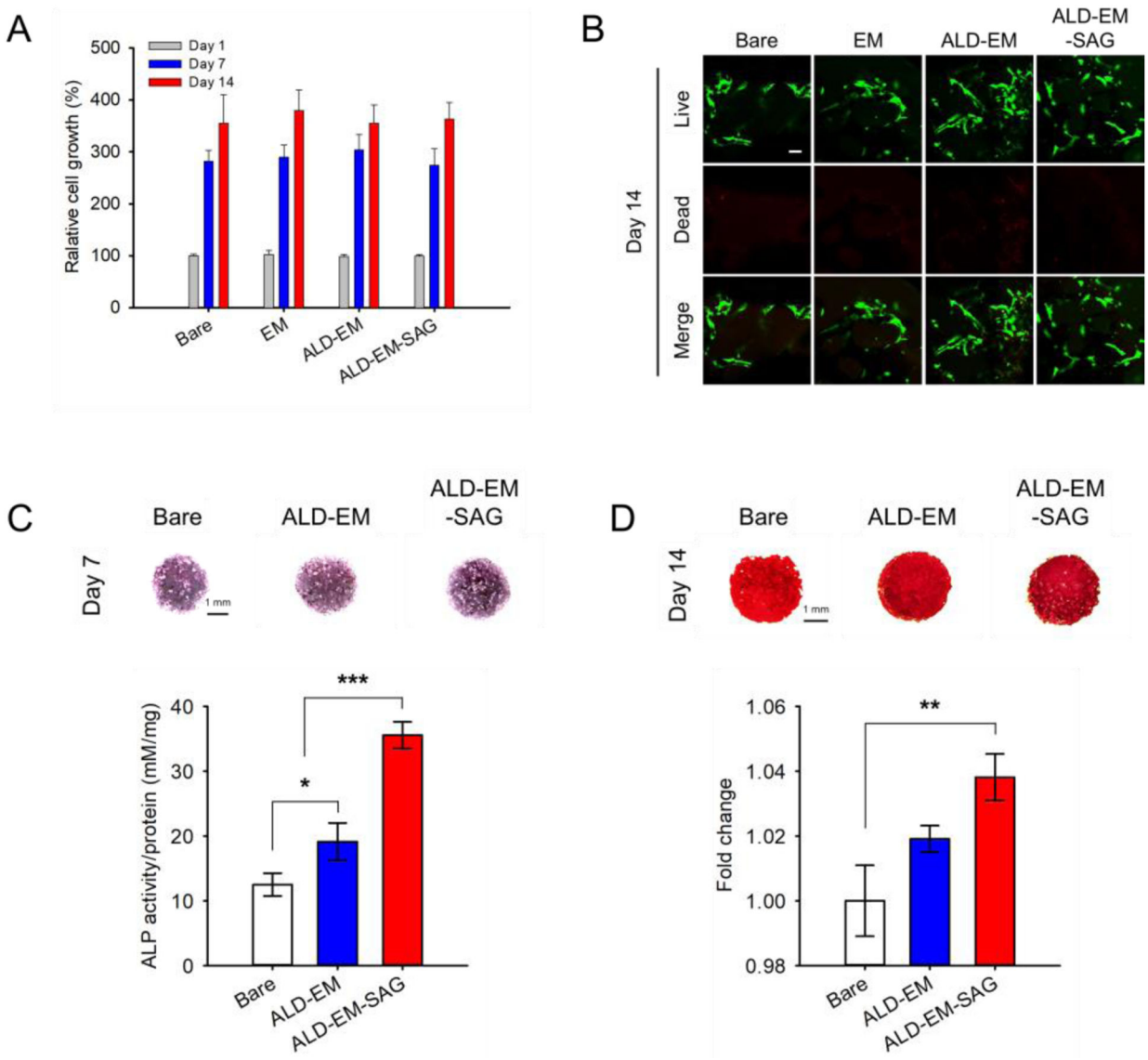

Figure 3. Cell adherence, proliferation, and bioactivity evaluation on EM-bound scaffolds.

A) *In vitro* cell proliferation after 1, 7, and 14 days. The value was normalized with bare HA-coated PLGA scaffold on day 1. B) Representative confocal fluorescence images of BMSCs stained with calcein AM (with live cells fluorescing green) and ethidium homodimer (with dead cells fluorescing red) on day 14. The scale bar indicates 100 μm. C) ALP staining and colorimetric quantification of BMSCs on scaffolds on day 4. D) Alizarin red S staining and quantified mineralized extracellular matrix of BMSCs on scaffolds on day 14. Data were presented as means ± standard deviation (n=3). *P < 0.05 **P < 0.01, ***P < 0.001, one-way ANOVA with Tukey's post hoc test. The scale bars indicate 1 mm in C and D.

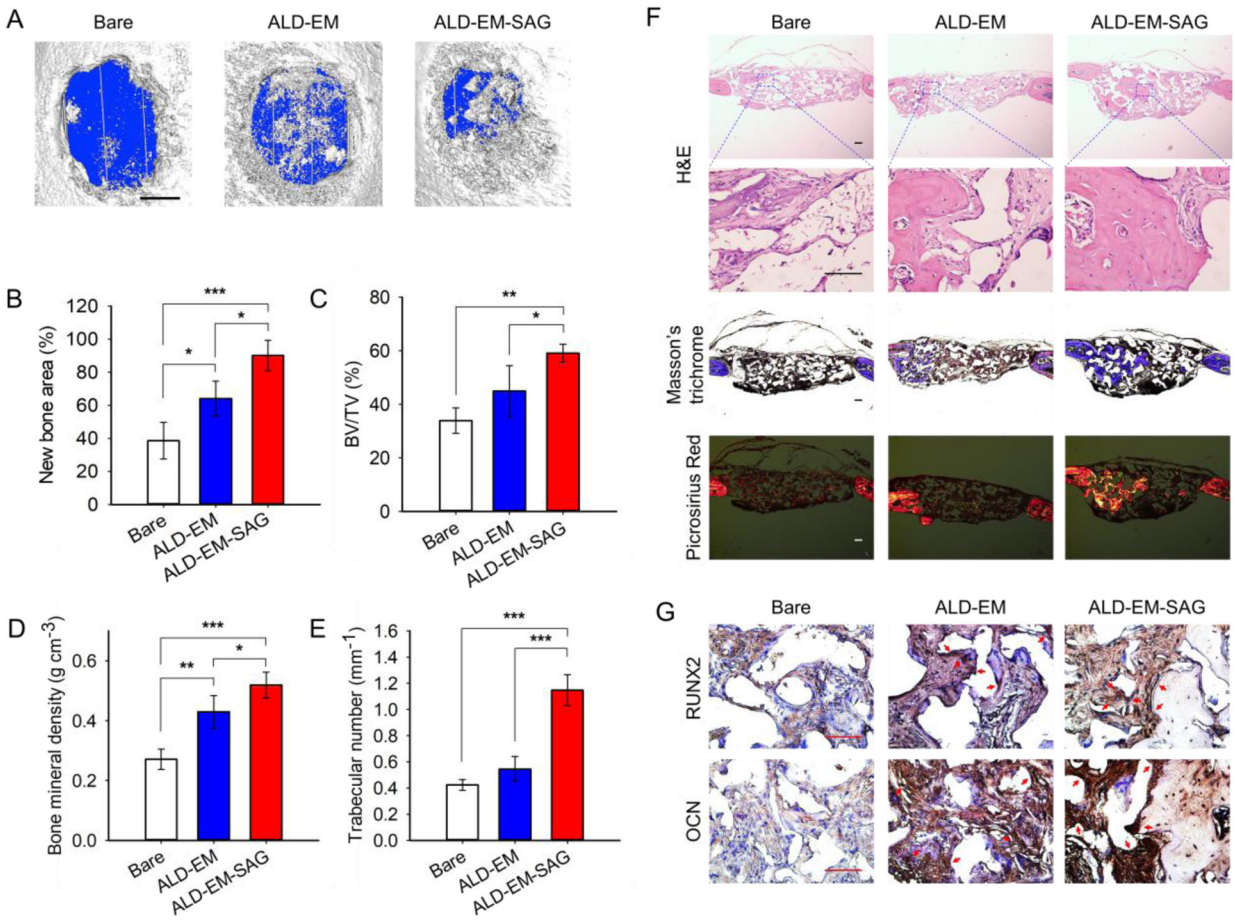

Figure 4. Effect of bone regeneration *in vivo* on calvarial defect following the implantation of EM-bound scaffolds.

A) Representative 3D reconstructed images of calvarial defect 12 weeks after the implantation of EM- or SAG-loaded EM (EM-SAG)-bound scaffolds taken with superficial view. The scale bar represents 1 mm in A. The quantified parameters of the regenerated bone, including B) new bone area, C) bone volume density (BV/TV; bone volume: BV; tissue volume: TV), D) bone mineral density, and E) trabecular number taken at the 3 mm diameter cylindrical defect. All data are presented as mean ± SD (n = 4). The statistical analyses were done with one-way ANOVA with Tukey's post hoc test; *p< 0.05, **p< 0.01, and ***p< 0.001. F) Histologic sections of calvarial decalcified sections stained with H&E, Masson's trichrome, and Picrosirius red after 12 weeks of implantation. G) Immunohistochemical analysis of Runt-related transcription factor 2 (RUNX2) and Osteocalcin (OCN) after 12 weeks of implantation. Brown color indicates stained RUNX2 and OCN in G. The scale bars indicate 100 μm in F and G. The red arrows indicate protein expression in G.

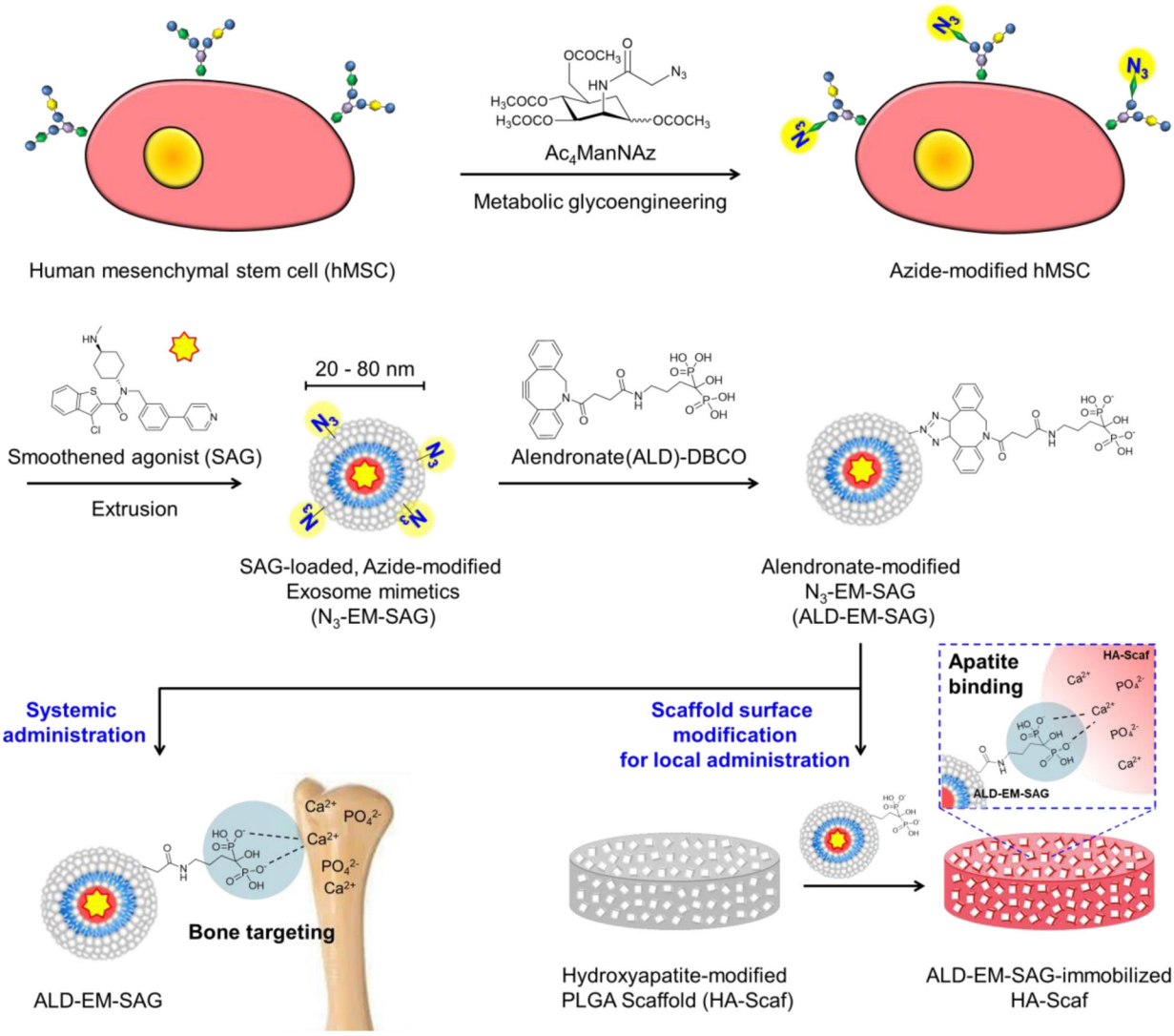

Scheme 1. Schematic illustration of bone-targeting exosome mimetics (EMs) engineered through bioorthogonal surface functionalization for bone regeneration.

The azides are generated on the surface of cells through metabolic glycoengineering. The drug (Smoothened agonist, SAG)-loaded EMs are fabricated by means of an extrusion method. Bone-targeting ligands (alendronate, ALD) are attached to the azides on the surface of EMs through bioorthogonal click chemistry. The resulting EMs (ALD-EM-SAG) can accomplish bone-targeting drug delivery and the surface engineering of biomaterial scaffolds for systemic and local bone regeneration.